

# Atomistic mechanisms of twin-twin interactions in Cu nanopillars

G. Sainath<sup>a,\*</sup>, Sunil Goyal<sup>a,b</sup>, A. Nagesha<sup>a,b</sup>

<sup>a</sup>Materials Development and Technology Division, Metallurgy and Materials Group, Indira Gandhi Centre for Atomic Research, Kalpakkam, Tamilnadu-603102, India

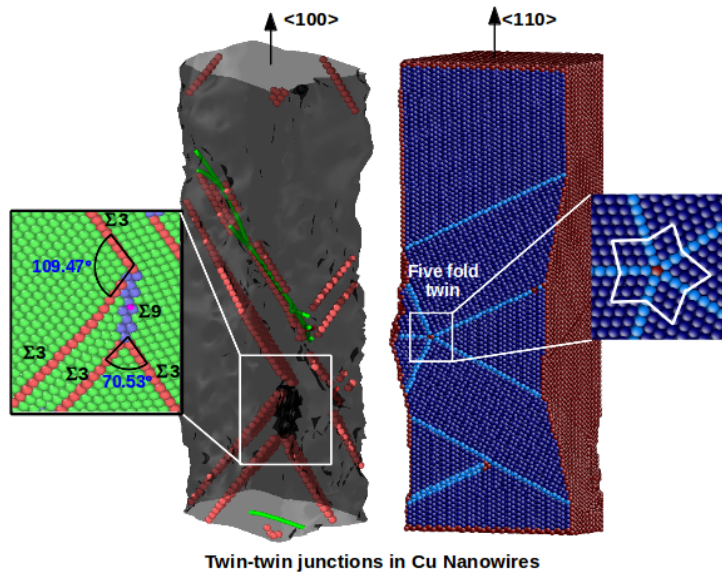
<sup>b</sup>Homi Bhabha National Institute, Indira Gandhi Centre for Atomic Research, Kalpakkam, Tamilnadu-603102, India

## Abstract

Twinning is an important mode of plastic deformation in metallic nanopillars. When twinning occurs on multiple systems, it is possible that twins belonging to different twin systems interact and forms a complex twin-twin junctions. Revealing the atomistic mechanisms of how twin-twin interactions lead to different twin junctions is crucial for our understanding of mechanical behaviour of materials. In this paper, we report the atomistic mechanisms responsible for the formation of two different twin-twin interactions/junctions in Cu nanopillars using atomistic simulations. One junction contains two twin boundaries along with one  $\Sigma 9$  boundary, while the other contains five twin boundaries (five-fold twin). These junctions were observed during the tensile deformation of  $[100]$  and  $[\bar{1}10]$  Cu nanopillars, respectively.

**Keywords:** Molecular Dynamics; Cu nanopillar; Twin boundaries; Dislocations; Twin junctions

## Graphical Abstract



\*Corresponding author

Email address: sg@igcar.gov.in or mohansainathan@gmail.com (G. Sainath)

## 1. Introduction

Many experimental and atomistic simulation studies have shown that twinning is an important mode of plastic deformation in FCC nanopillars [1, 2, 3] and nanocrystalline materials [4, 5]. Generally, twinning occurs in low stacking fault energy (SFE) materials such as Au and Cu under conditions that lead to high stresses, such as high strain rates, low temperatures and small size [6, 7]. Low SFE increases the separation between leading and trailing partials, which increases the barrier for full slip leading to the occurrence of twinning. In nanopillars, the occurrence of twinning has been explained in terms of different Schmid factors for leading and trailing partials [1]. Twinning occurs when the Schmid factor for leading partial is higher than the trailing partial [1]. This condition is readily met in  $\langle 100 \rangle$  nanopillar deforming under compression,  $\langle 110 \rangle$  and  $\langle 111 \rangle$  nanopillars under tension. As a result, numerous studies have reported twinning in these orientations and loading conditions [2, 8, 9, 10]. Further, when twinning occurs on limited twin systems, nanopillars undergo complete reorientation [10, 11], which also leads to sequential reorientation [12], shape memory and pseudo-elasticity. However, when twinning occurs on multiple twin systems, it is possible that the twins belonging to different twin systems interact and form a more complex twin-twin junctions. Compared to individual twin boundaries (TBs), twin-twin junctions are complex in nature and have a significant and distinct role on the physical and mechanical properties of materials. For example, the twin-twin junctions retard grain boundary migration and/or grain growth [13], causes detwinning [14], hinders the growth of existing twins and increases the strain hardening rate [15]. Such junctions can also influence the transport phenomena (ex. diffusion) along the grain boundaries [16] and thus influencing the high temperature properties of materials like creep. Further, twin boundaries forming a twin-twin junction can accommodate large shear strains and lead to rearrangement of grain boundary network [17, 18]. Therefore, characterizing the twin junctions or twin-twin interactions is of utmost importance in understanding the micro-structural evolution and deformation mechanisms, which in turn dictates the mechanical properties.

There are many studies which characterized the twin-twin interactions in bulk materials [19, 20]. For example, in Hadfield steel, it has been shown that, due to twin-twin interactions, the intersected region of two twins can form a second-order twin [19]. A second-order twin is a twin formed within an already twinned region of a crystal. Similarly, many grain boundary engineering studies have shown that, when two coherent TBs interact, either  $\Sigma 9$  or  $\Sigma 27$  boundary is observed at their intersection, i.e.,  $\Sigma 3 + \Sigma 3 = \Sigma 3^n$ , where  $n = 1, 2, 3, \dots$  [16, 21]. It shows that the  $\Sigma 3^n$  type grain boundaries are geometrically related to  $\Sigma 3$  boundaries. Twin-twin interactions/junctions have also been characterized in nanocrystalline materials [13, 18, 22]. Different twin junctions containing five, four, three and two TBs along with other grain boundaries have been observed. These junctions were characterized using the molecular dynamics simulations [13] and also using high resolution transmission microscopy (HRTEM) [18]. Twin junctions with more than five TBs are not feasible due to crystallographic restriction. Out of all these junctions, observation of five-fold twin has attracted significant attention not only in plastic deformation of materials but also in crystallography and crystal growth studies.

Like bulk and nanocrystalline materials, it is also important to understand the twin-twin interactions and junctions in nanopillars/nanoparticles, which show extensive twinning during deformation. However, surprisingly, there are no experimental reports of twin-twin interactions/junctions in nanopillars and also only a few simulation studies exist in characterizing the twin-twin junctions [23, 24]. These studies on nanopillars have shown only the formation of five-fold twins under the bending and torsional loading conditions [23, 24]. Further, most of the studies pertaining to the twin-twin interactions in bulk/nanocrystalline materials were experimental [18, 19, 20, 22], where it is difficult to obtain the atomistic details. In view of this, the aim of the present investigation is to characterize and provide the atomistic mechanisms of how twin-twin interactions can lead to different twin-twin junctions in Cu nanopillars. We report two different twin-twin interactions, one containing two TBs along with one  $\Sigma 9$  boundary and the other with five TBs (five-fold twin), which are observed during the deformation of Cu nanopillars. The detailed dislocation/atomistic mechanisms responsible for the formation of such junctions have been explained by taking the advantage of atomistic simulations.

## 2. Simulation Details

Single crystal Cu nanopillars oriented in  $[100]$  and  $[1\bar{1}0]$  axial directions were considered in this study.  $[100]$  nanopillar is enclosed by all  $\{100\}$  type side surfaces, while the  $[1\bar{1}0]$  nanopillar has  $(111)$  and  $(11\bar{2})$  as side surfaces. The model nanopillars had a square cross-section width ( $d$ ) varying in the range 5.0 - 21.5 nm. The pillar length was twice the cross-section width. No periodic boundary conditions were used in any direction. On these model nanopillars, tensile loading has been simulated using molecular dynamics (MD) simulations. All MD simulations were carried out in LAMMPS package [25] employing an EAM potential for Cu given by Mishin et al. [26]. This potential is widely used to study the deformation behaviour of Cu nanopillars [27, 28]. After initial construction of nanopillars, energy minimization was performed by conjugate gradient method to obtain a relaxed structure. Velocity verlet algorithm was used to integrate the equations of motion with a time step of 2 fs. Before applying tensile load, the relaxed nanopillars were equilibrated to a required temperature of 10 K in NVT ensemble. Following equilibration, the deformation was carried out in a displacement-controlled manner at constant strain rate of  $1 \times 10^8 \text{ s}^{-1}$  by imposing displacements to atoms along the nanopillar length that varied linearly from zero at the bottom fixed layer to a maximum value at the top fixed layer [28]. The visualization of TBs and dislocations is accomplished in AtomEye [29] and OVITO [30] using common neighbour analysis (CNA). Further, all over the manuscript the TB means  $\Sigma 3(111)$  coherent twin boundary.

## 3. Results and Discussion

### 3.1. Formation of $\Sigma 9$ boundary

Figure 1a shows a schematic of twin (Twin-1) approaching towards an already existing twin (Twin-2) in FCC material. As a result of their interaction, a  $\Sigma 9$  boundary forms at their intersection, which connects the

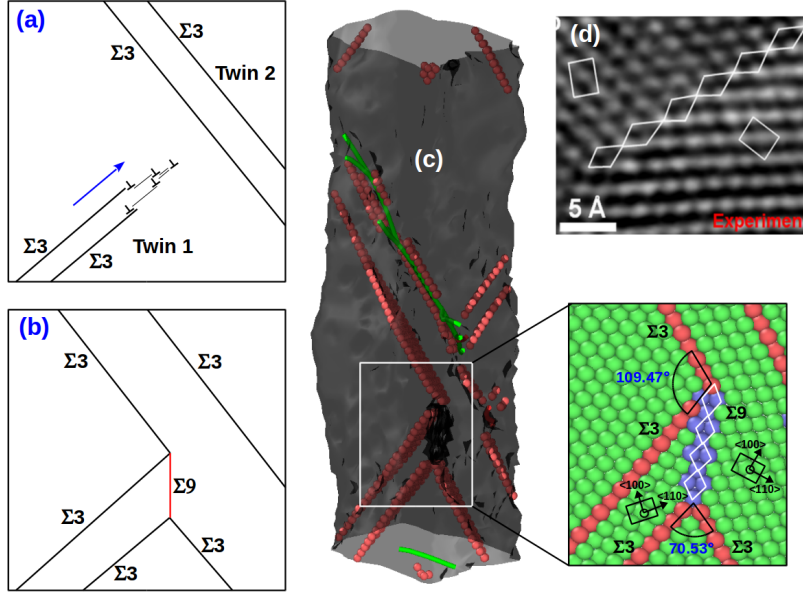


Figure 1: (a-b) A schematic showing twin-twin interactions resulting in the formation of a  $\Sigma 9$  boundary, (c) formation of a  $\Sigma 9$  boundary at twin-twin junction during the tensile deformation of  $[100]$  Cu nanopillar with  $d = 10$  nm, and (d) the structure of  $\Sigma 9$  boundary in nanocrystalline Pt observed using HRTEM by Wang et al. [18]. The atoms in Figure (c) and its subset are colored according to their CNA parameter; green = FCC, orange = HCP (TBs) and blue =  $\Sigma 9$  boundary. The continuum green lines are partial dislocations.

two  $\Sigma 3$ - $\Sigma 3$  junctions (Figure 1b). At one junction, the two  $\Sigma 3$  boundaries are at an acute angle ( $70.53^\circ$ ) to each other, while at other junction, they make an obtuse angle ( $109.47^\circ$ ). Interestingly, as shown in Figure 1c, a similar twin-twin interaction leading to the formation of a  $\Sigma 9$  boundary has been observed under the tensile loading of  $\langle 100 \rangle$  Cu nanopillar. The detailed atomic structure of the observed  $\Sigma 9$  boundary viewed along  $\langle 110 \rangle$  misorientation axis is shown in subset Figure 1c. It is interesting to see that the atomic structure of  $\Sigma 9$  boundary observed in the present investigation is quite similar to that observed using HRTEM (Figure 1d) in nanocrystalline Pt [18]. The misorientation angle (angle between  $\{110\}$  or  $\{100\}$  planes across the grain boundary) with respect to  $\langle 110 \rangle$  misorientation axis is found to be close to  $42^\circ$ , which is little higher than the theoretical value of  $38.94^\circ$  [31]. This difference in misorientation angle can be attributed to local stress concentration and also deformation induced lattice distortion [18], which are neglected while calculating the theoretical values. Further, it has been found that the  $\Sigma 9$  boundary in Cu nanopillar (Figure 1c) is parallel to one of the  $\{221\}$  planes. This abides well with the fact that the  $\Sigma 9$  boundary lies parallel to either  $\{114\}$  or  $\{122\}$  plane [31].

It is well known that when two  $\Sigma 3$  boundaries interact, either  $\Sigma 9$  or  $\Sigma 27$  boundary is observed at their intersection[21]. However, the detailed mechanism responsible for the formation of such higher order boundary is not well understood. Understanding this mechanism is important as it is known that the  $\Sigma 9$  boundary takes part in reconfiguration of the existing grain boundary network during the plastic deformation.

Figure 2 shows the detailed mechanism responsible for the formation of a  $\Sigma 9$  boundary at the intersection of two  $\Sigma 3$  boundaries. As shown in Figure 2a, an initial twin exists on plane  $\alpha = (111)$ . During deformation,

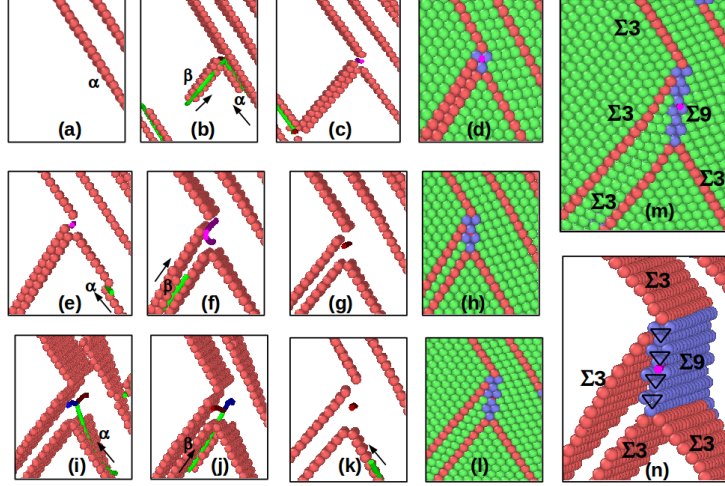


Figure 2: (a-l) A detailed dislocation mechanism responsible for the formation of a  $\Sigma 9$  boundary during the tensile deformation of  $[100]$  Cu nanopillar, and (m-n)  $\Sigma 9$  boundary with four structural units connecting two twin-junctions. All the atoms are colored according to their CNA parameter; green = FCC, orange = HCP (TBs) and blue =  $\Sigma 9$  boundary. The continuum green lines are partial dislocations and other color lines are stair-rod or grain boundary dislocations.

a new slip system on plane  $\beta = (\bar{1}11)$  gets activated by the glide of a partial dislocation (Figure 2b). With increasing strain, the partial dislocations on plane  $\alpha$  and  $\beta$  interact at the junction and forms a  $\frac{1}{6}[011]$  stair-rod dislocation as shown in Figure 2c-d. This reaction can be written as

$$\frac{1}{6}[12\bar{1}]\beta + \frac{1}{6}[\bar{1}\bar{1}2]\alpha \longrightarrow \frac{1}{6}[011]. \quad (1)$$

As shown in Figure 2d, this stair-rod dislocation is surrounded by three atomic rows (blue colour), which are neither FCC atoms nor stacking fault (HCP) atoms. These three atomic rows form one structural unit of a grain boundary. Following the formation of one structural unit, a twinning partial dislocation glides on plane  $\alpha$  (Figure 2e) and interacts with  $\frac{1}{6}[011]$  stair-rod dislocation (Figure 2f) according to the reaction

$$\frac{1}{6}[\bar{1}\bar{1}2]\alpha + \frac{1}{6}[011] \longrightarrow \frac{1}{6}[\bar{1}03]. \quad (2)$$

Here, the reaction violates the Frank rule which makes the  $\frac{1}{6}[\bar{1}03]$  dislocation highly unstable. As a result, this dislocation frequently dissociates (Figure 2f) and recombines according to the following reaction

$$\frac{1}{6}[\bar{1}03] \longrightarrow \frac{1}{6}[0\bar{1}\bar{1}] + \frac{1}{6}[\bar{1}14] \longrightarrow \frac{1}{6}[\bar{1}03]. \quad (3)$$

Interestingly, the  $\frac{1}{6}[\bar{1}03]$  dislocation formed via above recombination reaction minimises the energy, i.e., follows the Frank rule and also it is stable, unlike the previous one. Following recombination, another partial dislocation gliding on plane  $\beta$  interacts with  $\frac{1}{6}[\bar{1}03]$  dislocation and results in the formation of another new

stair-rod dislocation as shown in Figure 2g-h. This reaction can be written as

$$\frac{1}{6}[\bar{1}03] + \frac{1}{6}[12\bar{1}]\beta \longrightarrow \frac{1}{6}[022] \longrightarrow \frac{1}{3}[011]. \quad (4)$$

As shown in Figure 2h, the reactions (2) and (4) together adds one more structural unit to the grain boundary. The  $\frac{1}{3}[011]$  stair-rod dislocations formed at the end of reaction (4) lies in between these two structural units (Figure 2h) and, it is equivalent of two  $\frac{1}{6}[011]$  stair-rod dislocations ( $\frac{1}{3}[011] \longrightarrow \frac{1}{6}[011] + \frac{1}{6}[011]$ ), each at one structural unit. With further deformation, one more partial dislocation gliding on plane  $\alpha$  comes and interacts with  $\frac{1}{3}[011]$  stair-rod dislocation (Figure 2i) and results in the formation of a new dislocation as follows

$$\frac{1}{6}[\bar{1}\bar{1}2]\alpha + \frac{1}{6}[022] \longrightarrow \frac{1}{6}[\bar{1}14] \quad (5)$$

Here, the resultant  $\frac{1}{6}[\bar{1}14]$  dislocation forms a multiple of  $\frac{1}{18}[\bar{1}14]$ , which is one of the displacement shift complete (DSC) lattice dislocation of a  $\Sigma 9$  boundary [32]. Also, the reaction increases the energy, i.e., violates Frank criterion. However, the reaction is feasible due to the presence of high stresses within the grain boundary. Subsequently, one more partial dislocation gliding on plane  $\beta$  also comes and interacts with  $\frac{1}{6}[\bar{1}14]$  dislocation (Figure 2j) and results in the formation of  $\frac{1}{2}[011]$  stair-rod dislocation (Figure 2k-l) according to the following reaction

$$\frac{1}{6}[12\bar{1}]\beta + \frac{1}{6}[\bar{1}14] \longrightarrow \frac{1}{2}[011] \quad (6)$$

The reactions (5) and (6) together add one more structural unit to the grain boundary as shown in Figure 2l. Here, the  $\frac{1}{2}[011]$  stair-rod dislocation is equivalent of three  $\frac{1}{6}[011]$  stair-rod dislocations ( $\frac{1}{2}[011] \longrightarrow \frac{1}{6}[011] + \frac{1}{6}[011] + \frac{1}{6}[011]$ ), one at each structural unit. Thus, every interaction of partial dislocations emanating from two intersecting  $\{111\}$  planes contributes one  $\frac{1}{6}[011]$  stair-rod dislocation and adds one structural unit. In other words, the formation of  $\Sigma 9$  boundary just needs the repeated generation of  $1/6\langle 112 \rangle$  dislocation locks through two partial dislocation reactions as shown in Figures 2a-d. The continuous repetition of this process adds more and more structural units leading to an increase in  $\Sigma 9$  grain boundary length (Figure 2m-n). These results provide the direct evidence to the fact that  $\Sigma 9$  boundary is an array of  $\frac{1}{6}[011]$  type stair-rod dislocations as suggested by Zhu and co-workers [33].

### 3.2. Formation of five-fold twin

Five-fold twin is basically a junction of five different TBs meeting at one point and it exhibits an interesting five-fold symmetry. Twin-twin interactions leading to the formation of five-fold twin during the tensile deformation of  $\langle 110 \rangle$  Cu nanopillar is shown in Figure 3. Initially, the two twins (twin-1 and twin-2) grow on two different planes (Figure 3a) and as result of their interaction at the nanopillar corner, a five-fold twin forms at the intersection of two leading TBs (Figure 3b). Similar to the present observation, few studies in the literature have reported the formation of five-fold twins in nanopillars under bending and torsional

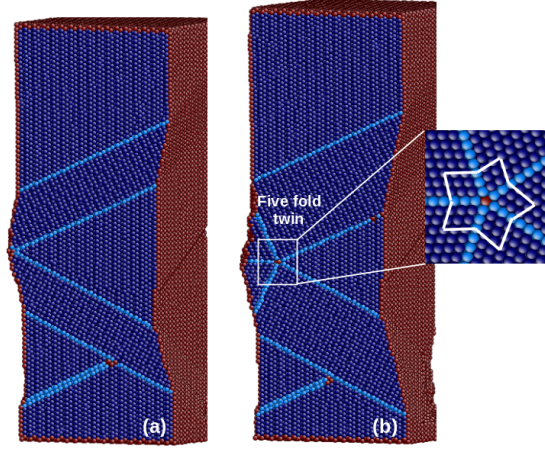


Figure 3: Twin-twin interactions leading to the formation of five-fold twin during the tensile deformation of  $\langle 110 \rangle$  Cu nanopillar with  $d = 7.2$  nm. (a) Two twins interacting at the nanopillar corner and (b) five-fold twin formed at the intersection of two twin boundaries near nanopillar corner. The atoms are colored according to their CNA parameter; dark blue = FCC, light blue = HCP (TBs) and red = surface or dislocation core atoms.

loading conditions [23, 24]. However, it has never been observed during the uniaxial loading of nanopillars. Initially, it has been proposed that the essential requirement for the formation of five-fold twin are (i) large shear stress to activate multiple slip systems and (ii) variation in stress orientation such that several partials with different orientations can be nucleated [34, 35]. Generally, torsion and bending tests provide such conditions. Accordingly, it was claimed that the uniaxial stress conditions may not lead to five-fold twins [34]. However, the observation of five-fold twin close to nanopillar corner as shown in Figure 3b indicates that these two conditions were readily satisfied at nanopillar corners even under tensile loading. Generally, the stress is high at nanopillars corners and also there is a possibility of change in stress orientation. Similar to the present study, Cao and Wei [36] have also reported the formation of five-fold twins under tensile loading of nanocrystalline Cu and suggested that the stress state within a small region is always a complex one even under uniaxial conditions.

In literature, different mechanisms have been suggested for the formation of five-fold twin. In nanocrystalline materials, it has been shown that the migration of grain boundary segment is responsible for the formation of five-fold twin [13]. Similarly, Bringa et al. [35] have reported that multiple emissions of partial dislocations from the grain boundaries due to high local stresses leads to the formation of five-fold twin. In nanopillars, Zheng et al. [23] have demonstrated that an intermediate icosahedral phase facilitates the formation of five-fold twin. In Cu nanoparticles, the TEM observations indicate that initially the lattice gets distorted and this distorted portion acts as a partial dislocation source [37]. The glide of these partial dislocations induces a layer-by-layer migration of TBs resulting in a standard five-fold twin [37]. Thus, there lies a great ambiguity over the formation of five-fold twin in nanopillars/nanocrystalline materials.

The detailed atomistic mechanism responsible for the formation of five-fold twin in the present study is shown in Figure 4. Different from previous observations, five-fold twin directly nucleates from the distorted lattice formed at nanopillar corner. During initial straining, two TBs making an angle of  $70.53^\circ$  with respect

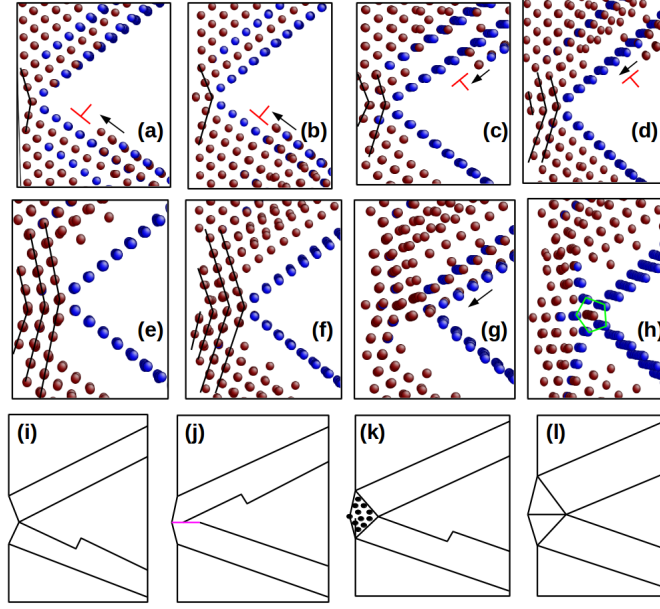


Figure 4: (a-h) The detailed atomistic mechanism responsible for the formation of five-fold twin during the tensile deformation of  $\langle 110 \rangle$  Cu nanopillar. The same process is summarized schematically in (i-l). The atoms in Figure (a-h) are colored according to their CNA parameter; blue = HCP (TBs) and red = surface or dislocation core atoms. The FCC atoms are not shown for clarity.

to each other meet at nanopillar corner (Figure 3a and 4a). Following this, a partial dislocation glides on one of the TBs, which drives the twin junction by one atomic step away from corner (Figure 4a-b). This process of partial dislocation glide continues to occur on two intersecting TBs and makes the twin junction to move inwards, i.e., away from nanopillar corner (Figure 4a-d). As a result, the atoms/planes between nanopillar corner and twin junction change to disorder/non-closed pack state (Figure 4c-f). In other words, the lattice gets distorted locally near nanopillar corner due to twin-twin interactions. With increasing strain, as this distorted lattice is highly unstable, a five-fold twin nucleates from the distorted region due to atomic readjustments (Figure 4g-h). These atomic adjustments were mainly aided by the partial dislocation movements on the existing TBs. As a result, a clear five-fold twin can be seen in Figure 4h. This complete process is summarized schematically in Figures 4i-l. Since the angle between any  $\{111\}$  planes in FCC system is  $70.53^\circ$ , a five-fold twin leaves a gap of  $7.35^\circ$  ( $360 - 5 \times 70.53$ ). However, such gap is accommodated by the elastic strain within the twinned regions. It has been further observed that, with increasing deformation, the centre point of five-fold twin move towards the nanopillar interior due to partial dislocation glide on TBs. Thus, the five-fold twin under the tensile loading of Cu nanopillars nucleates from the distorted lattice formed close to nanopillar corner. The distorted lattice at the corner is formed due to the continuous glide of partial dislocations on two intersecting TBs. This process of five-fold twin formation is remarkably different from that reported in nanocrystalline materials [13, 35] and other nanopillars/nanoparticles [23, 37]. In previous studies, the involvement of grain boundaries/partial dislocations/icosahedral phase was needed for five-fold twin formation, whereas the present study shows that the atomic shuffling at the intersection point

of two existing twin boundaries can also results in five-fold twin formation.

### 3.3. Size effects and stress-strain behaviour

The above mentioned twin-twin junctions, i.e.,  $\Sigma 3$ - $\Sigma 3$ - $\Sigma 9$  and five-fold twin, have been observed in all the nanopillars with size ( $d$ ) in the range 5.0 - 21.5 nm. However, the area (or structural units in Figure 2n) of the newly formed  $\Sigma 9$  boundary is different in different nanopillars. The observed number of structural units as shown in Figure 2n varied from two to maximum of six. On the contrary, the five-fold twin has not shown any remarkable differences among nanopillars of different size. However, it is of significant interest to understand the size dependence of twin-twin junctions in nanopillars and nanocrystalline materials over a wide range of sizes. To this, Cao et al. [22] have analysed the formation frequency of different twin-twin junctions with respect to the grain size in nanocrystalline Cu. It has been found that formation frequency increases with decreasing grain size, then reaches a peak around 35-45 nm, and again decreases at lower grain sizes [22]. Similar study is needed in nanopillars to understand the size dependence of twin-twin junctions.

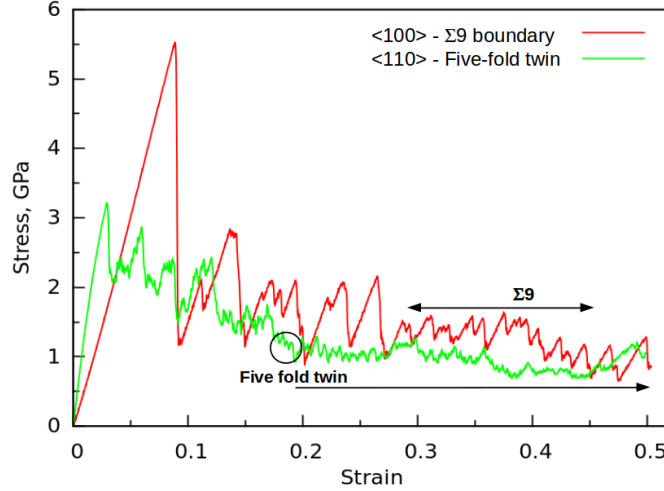


Figure 5: The stress-strain behaviour of  $[100]$  and  $[1\bar{1}0]$  Cu nanopillars under tensile loading at 10 K. In  $[100]$  nanopillar, the formation of  $\Sigma 9$  boundary has been observed, while in  $[1\bar{1}0]$  nanopillar, a five-fold twin was observed. The strain values at which the twin-twin interactions were observed are indicated.

Figure 5 shows the stress-strain behaviour of  $[100]$  and  $[1\bar{1}0]$  Cu nanopillars with  $d = 10$  nm, where the formation of  $\Sigma 9$  boundary and five-fold twin was observed in respective orientations. Following an initial linear elastic deformation, both the nanopillars show an extensive plastic deformation characterized by flow stress fluctuations along with an average decrease in flow stress. The strain range over which the above mentioned twin-twin interactions were observed is highlighted in Figure 5. The formation of  $\Sigma 9$  boundary has been observed over a strain range of 0.3-0.45. Over this strain range, the area of the grain boundary increases gradually with increasing strain beginning with one structural unit. On the other hand, the five-fold twin boundary has formed at a strain ( $\varepsilon$ ) value of 0.18 and remained in the nanopillar till the strain value of more than 0.5. During this period ( $\varepsilon = 0.18 - 0.5$ ), the gradual movement of centre of five-fold twin has been observed.

#### 4. Conclusions

In summary, molecular dynamics simulations performed on  $[100]$  and  $[1\bar{1}0]$  Cu nanopillars indicate that multiple twin systems activate and interactions among themselves leads to complex twin-twin junctions. The atomistic mechanisms responsible for the formation of such twin-twin junctions have been revealed in detail. During the tensile deformation of  $[100]$  nanopillar, a twin junction containing two TBs along with one  $\Sigma 9$  boundary, i.e.,  $\Sigma 3$ - $\Sigma 3$ - $\Sigma 9$  junction, has been observed. At this junction, the  $\Sigma 9$  boundary is added unit by unit by an interesting partial dislocation reaction at the intersection of two TBs. This process is quite similar to the experimental observation in nanocrystalline Pt [18]. However, due to the advantage of atomistic simulations, the present study provides the detailed picture of dislocation interactions at the twin-twin junction. This understanding help us to explain how the  $\Sigma 9$  boundary takes part in reconfiguring the grain boundary network during the plastic deformation of polycrystalline materials. On the other hand, in  $[1\bar{1}0]$  nanopillar, a junction of five different TBs meeting at one point, i.e., five-fold twin has been observed. This five-fold twin nucleates from the distorted lattice formed close to nanopillar corner. The distorted lattice at the corner is formed due to the continuous glide of partial dislocations on the two intersecting TBs. This observation sheds a new light on the formation mechanism of five-fold twin in nanopillars.

#### References

- [1] C.R. Weinberger, W. Cai, J. Mater. Chem. 22 (2012) 3277-3292.
- [2] S. Lee, J. Im, Y. Yoo, E. Bitzek, D. Kiener, G. Richter, B. Kim, S.H. Oh, Nature Comm. 5 (2014) 3033.
- [3] J. Wang, S.X. Mao, Extr. Mech. Lett. 8 (2016) 127-139.
- [4] L. Wang, P. Guan, J. Teng, P. Liu, D. Chen, W. Xie, D. Kong, S. Zhang, T. Zhu, Z. Zhang, E. Ma, M. Chen, X. Han, Nature Commun. 8 (2017) 2142.
- [5] L. Wang, K. Du, C. Yang, J. Teng, L. Fu, Y. Guo, Z. Zhang, X. Han, Nature Commun. 11 (2020) 1167.
- [6] Q. Yu, L. Qi, K. Chen, R.K. Mishra, J. Li, A.M. Minor, Nano Lett. 12 (2012) 887.
- [7] D. Kiener, A.M. Minor, Nano Lett. 11 (2011) 3816.
- [8] A. Cao, E. Ma, Acta Mater. 56 (2008) 4816-4828.
- [9] H. Zheng, A. Cao, C.R. Weinberger, J.Y. Huang, K. Du, J. Wang, Y. Ma, Y. Xia, S.X. Mao, Nature Commun. 1 (2010) 144.
- [10] P. Rohith, G. Sainath, B.K. Choudhary, Comput. Cond. Matt. 16 (2018) e00330.
- [11] H.S. Park, K. Gall, J.A. Zimmerman, Phys. Rev. Lett. 95 (2005) 255504.
- [12] P. Rohith, G. Sainath and B. K. Choudhary, Phil. Mag. Lett. 97 (2017) 408-416.

- [13] S.L. Thomas, A.H. King, D.J. Srolovitz, *Acta Mater.* 113 (2016) 301-310.
- [14] G. Sainath, Sunil Goyal and A. Nagesha, *Crystals* 10 (2020) 366.
- [15] H. El Kadiri, J. Kapil, A.L. Oppedal, L.G. Hector, S.R. Agnew, M. Cherkaoui, S.C. Vogel, *Acta Mater.* 61 (2013) 3549-3563.
- [16] V. Randle, *J. Microscopy*, 222 (2006) 69-75.
- [17] L. Wang, D. Kong, Y. Zhang, L. Xiao, Y. Lu, Z. Chen, Z. Zhang, J. Zou, T. Zhu, X. Han, *ACS Nano* 11 (2017) 12500-12508.
- [18] L. Wang, T. Jiao, W. Yu, S. Xuechao, X. Sisi, M. Shengcheng, Y. Guanghua, Z. Zec, Z. Jind, H. Xiaodong, *Ultramicroscopy* 195 (2018) 69-73.
- [19] C. Efstathiou, H. Sehitoglu, *Acta Mater.* 58 (2010) 1479-1488.
- [20] P. Mullner, C. Solenthaler, M. Speidel, *Acta Metall. Mater.* 42 (1994) 1727-32.
- [21] V. Randle, G. Owen, *Acta Mater.* 54 (2006) 1777-1783.
- [22] Z.H. Cao, L.J. Xu, W. Sun, J. Shi, M.Z. Wei, G.J. Pan, X.B. Yang, J.W. Zhao, X.K. Meng, *Acta Mater.* 95 (2015) 312-323.
- [23] Y.G. Zheng, H.W. Zhang, Z. Chen, L. Wang, Z.Q. Zhang, J.B. Wang, *Appl. Phys. Lett.* 92 (2008) 041913.
- [24] X. Tian, J. Cui, C. Zhang, Z. Ma, R. Wan, Q. Zhang, *Comput. Mater. Sci.* 83 (2014) 250-254.
- [25] S. Plimpton, *J. Comp. Phy.* 117 (1995) 1-19.
- [26] Y. Mishin, M.J. Mehl, D.A. Papaconstantopoulos, A.F. Voter, J.D. Kress, *Phys. Rev. B*, 63 (2001) 1-16.
- [27] H. Liang, M. Upmanyu, H. Huang, *Phys. Rev. B* 71 (2005) 26
- [28] G. Sainath, B.K. Choudhary, *Phys. Lett. A* 379 (2015) 1902-1905.
- [29] J. Li, *Modell. Simul. Mater. Sci. Eng.* 11 (2003) 173.
- [30] A. Stukowski, *Modell. Simul. Mater. Sci. Eng.* 18 (2009) 015012.
- [31] J.D. Rittner, D.N. Seidman, *Phys. Rev. B* 54 (1996) 6999-7015.
- [32] H. Foll, Lecture Notes on “Defects in Crystals”, Faculty of Engineering, University of Kiel, [https://www.tf.uni-kiel.de/matwis/amat/def\\_en/kap\\_7/backbone/r7\\_2\\_1.html](https://www.tf.uni-kiel.de/matwis/amat/def_en/kap_7/backbone/r7_2_1.html)
- [33] Y.T. Zhu, J. Narayan, J.P. Hirth, S. Mahajan, X.L. Wu, X.Z. Liao, *Acta Mater.* 57 (2009) 3763-3770.

- [34] Y.T. Zhu, X.Z. Liao, R.Z. Valiev, Appl. Phys. Lett. 86 (2005) 103112.
- [35] E.M. Bringa, D. Farkas, A. Caro, Y.M. Wang, J. McNaney, R. Smith, Scr. Mater. 59 (2008) 1267-1270.
- [36] A.J. Cao, Y.G. Wei, Appl. Phys. Lett. 89 (2006) 041919.
- [37] Z. Deng, J. Luo, W. Yuan, W. Xi, Scr. Mater. 169 (2019) 42-45.